

1 **Topographic modulation on the layered circulation in South China Sea**

2
3
4
5
6
7
8
9
10
11
12
13
14
15

Qibang Tang^{1,2}, Zhongya Cai^{1,2}, Zhiqiang Liu³

1 State Key Laboratory of Internet of Things for Smart City, Department of Ocean Science and Technology, University of Macau, China

2 Centre of Ocean Research in Hong Kong and Macau (CORE), Hong Kong, China

3. Department of Ocean Science and Engineering and Center for Complex Flows and Soft Matter Research, Southern University of Science and Technology, Shenzhen, China

Correspondence to: Zhongya Cai (zyc@um.edu.mo)

16

17 **Abstract:** The South China Sea (SCS) is the largest semi-enclosed marginal sea in western
18 Pacific. It exhibits a unique vertically rotating cyclonic, anticyclonic, and cyclonic circulation
19 in its upper, middle, and deep layers. Over slope topography, these layered currents interact and
20 significantly shape the structure and intensity of the basin circulation. In this study, we employ
21 process-oriented numerical simulations to investigate how upper-layer processes, characterized
22 by greater magnitude and variability, influence the layered circulation over the irregular
23 topographic slope. The simulations reveal that stronger upper intrusion from open ocean
24 directly enhances upper layer circulation, which subsequently strengthens the middle and the
25 deep slope currents. Vorticity dynamics illustrate that changes in the middle and deep slope
26 current are largely related to the vertical stretching (ζ_{DIV}) induced by bottom geostrophic
27 cross-isobath transport (CGT_b). As the upper-layer cyclonic slope current intensifies, it
28 modulates the bottom pressure distribution, resulting in stronger negative ζ_{DIV} predominantly
29 over the northwestern slope to intensify the middle anticyclone slope current. Similarly, for the
30 deep cyclonic slope current, the CGT_b maintains downwelling in the northern part and
31 upwelling over the southern slope. Over the southern slope, the strengthening of the positive
32 CGT_b is induced by the increment of the advection of relative vorticity and planetary vorticity
33 in water column, in which the middle layer has important contribution, but the upper layer has
34 a minimal impact. Conversely, on the northern slope, the strengthening of the negative CGT_b is
35 primarily influenced by the upper layer.

36

37 **Keywords:** Circulation dynamics; Layered circulation; Process-oriented simulation;
38 Topographic modulation; Vertical coupling

39

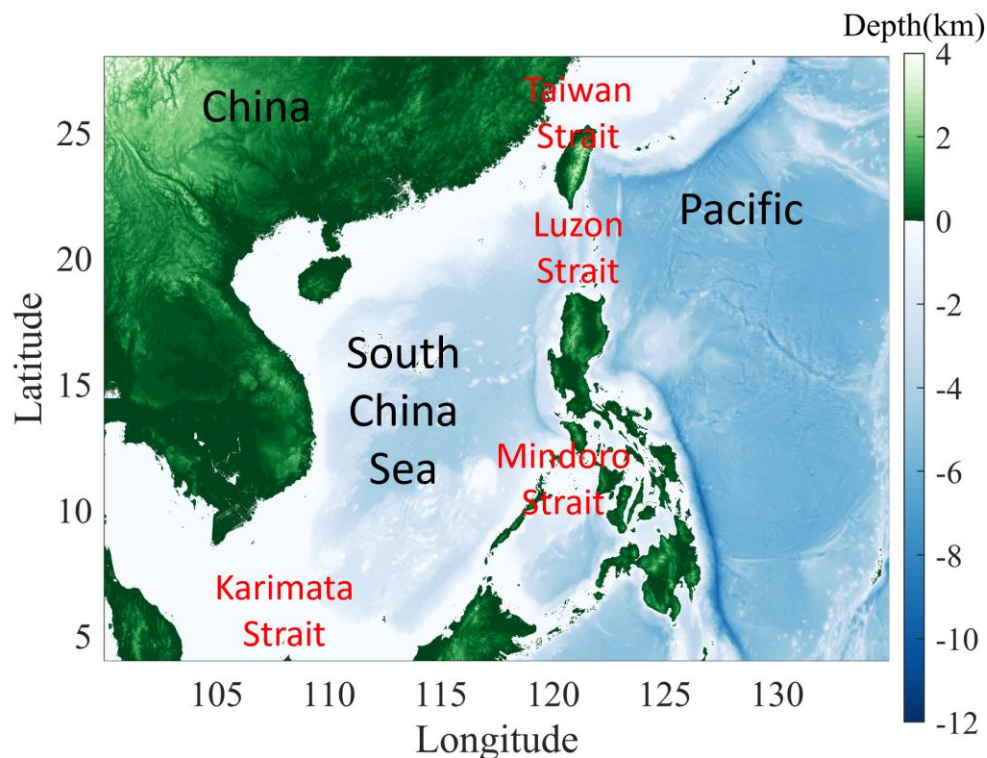
40 1. Introduction

41
42 Marginal seas circulation plays crucial role in the mass transport and regional climate
43 dynamics, with circulation patterns being strongly influenced by their unique topographic
44 features (Millot 1999, Omstedt, Elken et al. 2004, Oey, Ezer et al. 2005, Gan, Li et al. 2006,
45 Johns and Sofianos 2012). This topographic regulation results in intricate layered slope currents
46 that flow in different directions at various depths (Yuan 2002, Wang, Xie et al. 2011, Lan, Zhang
47 et al. 2013, Gan, Kung et al. 2022). These layered currents interact over slope topography,
48 significantly shaping the structure and intensity of the overall circulation (Gan, Liu et al. 2016,
49 Quan and Xue 2018). For instance, in the Gulf of Mexico, loop current eddies influence not
50 just the upper-layer circulation but also the deep flow, illustrating the importance of vertical
51 coupling in transferring energy and variability to deeper currents (Tenreiro, Candela et al. 2018).
52 Understanding these dynamics helps elucidate the behavior of marginal sea's circulation (Liang,
53 Spall et al. 2017, Zhu and Liang 2020, Olvera-Prado, Moreles et al. 2023).

54 The South China Sea (SCS) is the largest semi-enclosed marginal sea located in the
55 tropical region. It exhibits a unique mean cyclonic, anticyclonic, and cyclonic (CAC)
56 circulation in its upper, middle, and deep layers (Wang, Xie et al. 2011, Shu, Xue et al. 2014,
57 Lan, Wang et al. 2015, Gan, Liu et al. 2016, Zhu, Sun et al. 2017). The strong upper layer
58 circulation is driven by the Asia monsoon and Kuroshio intrusion from Luzon Strait (LS), while
59 the middle and deep circulations are maintained by the outflux and deep intrusion through LS,
60 respectively. Based on current understanding, the upper-layer influx through the Luzon Strait
61 (LS) is induced by the Kuroshio Current as it passes through the strait (Nan et al., 2015). The
62 middle-layer outflux and deep-layer intrusion, on the other hand, are largely driven by density
63 differences caused by contrasting turbulent mixing intensities (e.g., Tian et al., 2009; Zhu et al.,
64 2019; Zhou et al., 2023). Over the slope topography, the CAC circulation affects each other
65 through the vertical coupling among them (Shu, Wang et al. 2018). For example, the study of
66 Quan and Xue (2018) demonstrated that perturbations in the upper layer can transit through the
67 water column and affect deeper circulation by altering layer thickness. This coupling is
68 particularly evident over the strong boundary current that in the northern basin and along the
69 western boundary. Numerical experiments by Wang et al. (2018) suggest that, although the
70 basin-scale circulation is primarily driven by the LS overflow, upwelling patterns are essential
71 in shaping the detailed structure of the deep-water circulation. Similar processes have been
72 observed in other marginal seas as well (e.g., Testor et al., 2018; Wang et al., 2024; Xu et al.,
73 2009; Olvera-Prado, Moreles et al. 2023).

74 Despite advances in understanding the major features of mean layered circulation, the
75 response of this circulation to changes in external forcings—particularly the strong upper ocean

76 processes—and the specific mechanisms involved remain poorly understood. A comprehensive
77 understanding of how topographically modulated vertical coupling over basin slopes influences
78 the structure and intensity of mean circulation is crucial for exploring the long-term evolution
79 of marginal sea circulation. For instance, Kuroshio intrusion has been observed to weaken with
80 decadal variations, while upper ocean currents have shown acceleration in response to a
81 warming climate (Peng et al., 2022; Chen et al., 2019; Nan et al., 2013). How the layered
82 circulation in marginal seas responds to these changes remains unclear. This study employs
83 process-oriented simulations to elucidate how upper-layer processes, which exhibit greater
84 intensity and variability, influence layered circulation over the curved bottom slope in the SCS.
85 The paper is organized as follows: Section 2 explains the configuration of the simulation.
86 Section 3 offers the response of layered slope current intensity to the changes of the upper
87 circulation. Section 4 explores the underlying physical mechanisms. Finally, Section 5 provides
88 a summary of our findings.



89
90 **Figure1.** Location and bathymetry (km) of the South China Sea, showing Luzon Strait, Taiwan
91 Strait, Mindoro Strait, and Karimata Strait.

92
93

94 2. Methodology

95 Based on the Regional Ocean Modeling System (ROMS) (Shchepetkin & McWilliams,
96 2005), we performed a three-dimensional process-oriented simulation in this study (Cai et al.,
97 2023). The model setup included a circular basin on the west representing the SCS and a

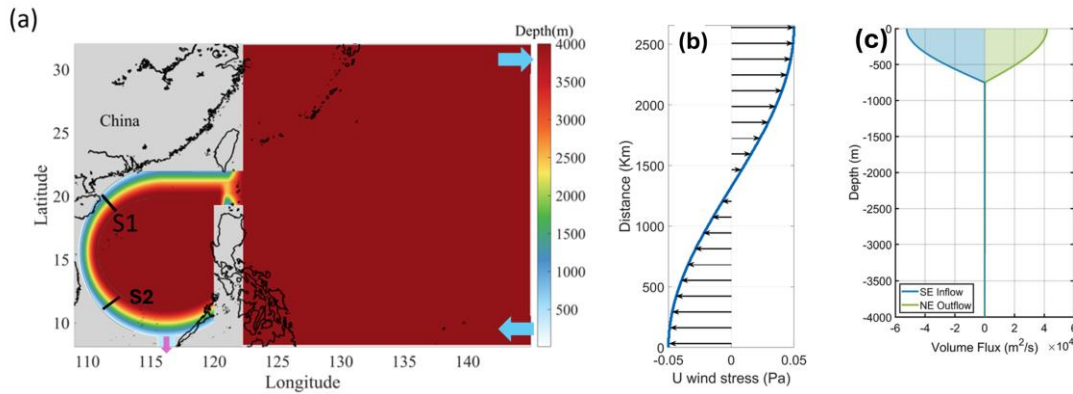
98 rectangular basin on the east representing the Western Pacific Ocean. The slope in the SCS
99 increases from 400 to 4000 m and the central basin has the depth of 4000 m. The SCS and
100 Pacific basins were connected by a narrow strait (representing the LS) with a depth of 2500 m.

101 The model employed a uniform horizontal grid with a 5 km resolution, and the vertical
102 structure utilized stretched, terrain-following coordinates with 30 layers (Song and Haidvogel
103 1994) were adopted with 30 layers. Near the surface and bottom boundaries, the vertical
104 resolution is refined with spacing of approximately 0.01. In the upper layer, an influx of 25 Sv
105 and an outflux of 20 Sv were specified at the southeastern and northeastern boundaries of the
106 open ocean, respectively (Figure 2c). The SCS was opened to the south with the depth of 400
107 m (Figure 2a), to allow the upper-layer intrusion to develop intrinsically during the simulation.
108 To simulate the density differences and exchange currents in the middle and deep layers of the
109 LS, the model incorporated variable contrasting mixing coefficients (K_v) between the SCS and
110 the Western Pacific Ocean (Tian, Yang et al. 2009, Yang, Zhao et al. 2016). In the SCS and the
111 western half of the LS, K_v values were set as $5 \cdot 10^{-4} m^2 s^{-1}$ between 500 and 1,500 m, $2 \cdot$
112 $10^{-3} m^2 s^{-1}$ below 1,500 m, and $5 \cdot 10^{-3} m^2 s^{-1}$ in the layer 500 m from the bottom. In the upper
113 500 m of SCS and LS, and throughout the entire water column of the open ocean, a background
114 K_v of $2 \cdot 10^{-5} m^2 s^{-1}$ was applied. The K_v was designed based on observational work by Yang
115 et al. (2016) and estimations by Wang et al. (2017) to form the circulation in the semi-enclosed
116 middle and deep layers. Then, simulations were conducted to explore the response of the
117 layered slope current, particularly in the semi-enclosed middle and deep layers, to changes in
118 the upper-layer circulation. A zonal wind stress with meridional variations was applied over
119 the open ocean, while the atmospheric buoyancy flux over the SCS was simplified by setting it
120 to zero. This model simplifies the configurations to focus on the fundamental dynamics of the
121 system. While these simplifications are essential for isolating key mechanisms, they may not
122 capture the complexity of real-world conditions, potentially limiting its quantitative
123 applicability to realistic processes.

124 The model was initialized with horizontally uniform temperature and salinity profiles
125 derived from the mean data of the World Ocean Atlas, averaged over the region west of the LS.
126 The simulation ran for 25 years, with the analysis was conducted on the results from the final
127 5 years average after the layered circulation reached a stable state.

128

129



130

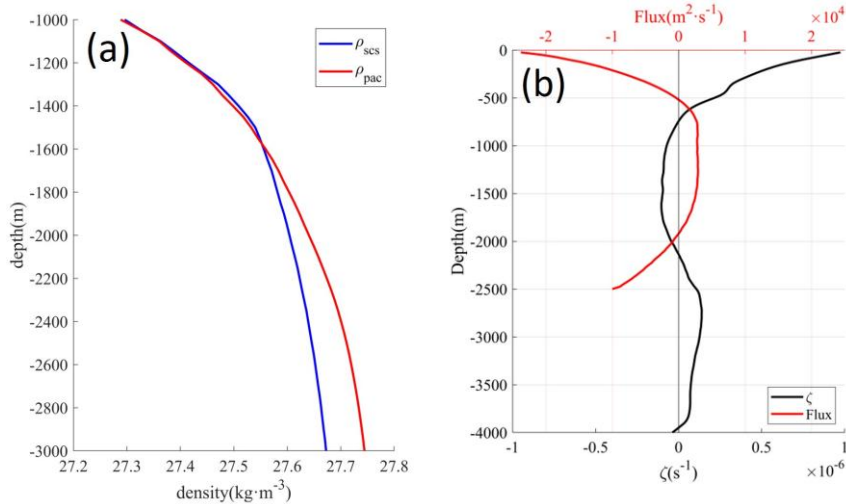
131

132 Figure 2. (a) The topography and geometry used in the idealized process-oriented simulation.
 133 The black lines show the realistic surrounding coastline. S1 and S2 are two vertical sections for
 134 showing slope current. (b) Distribution of the wind stress. (c) Vertical profile of the volume
 135 inflow/outflux (m²/s) through the southern/northern part of the eastern boundary
 136

136

137 3. Results

138 In the LS, the influx occurs in the upper and deep layers, while the outflow occurs in the
 139 middle layer between them (Figure 3b). The upper intrusion is intrinsically linked to the western
 140 boundary current in the open ocean, i.e. Kuroshio Current. In the middle and bottom layers, the
 141 exchange currents are primarily related to the density differences between the South China Sea
 142 (SCS) and the Pacific. Although the initial temperature and salinity distributions are horizontally
 143 uniform, the intensified turbulent mixing within the deep SCS basin gradually leads to a density
 144 difference between the two sides of the LS. Specifically, the deep SCS exhibits lower density
 145 compared to the Pacific basin (Figure S1). Under the density difference, the westward pressure
 146 gradient was formed that drives the deep intrusion from the open ocean towards the SCS. Those
 147 features are consistent with established understandings from previous studies (e.g., Wang, Xie
 148 et al. 2011, Zhu et al., 2017, 2019; Cai, Chen et al. 2023; Zhou et al., 2023). Associated with
 149 the simulated layered exchanging current, the layered circulations developed inside the SCS
 150 basin. The upper, middle, and deep layers exhibit circulation in cyclonic, anticyclonic, and
 151 cyclonic directions, respectively (Figure S1). The horizontally averaged vorticity features with
 152 the positive-negative-positive values in the respective depth of the basin (Figure 3b).



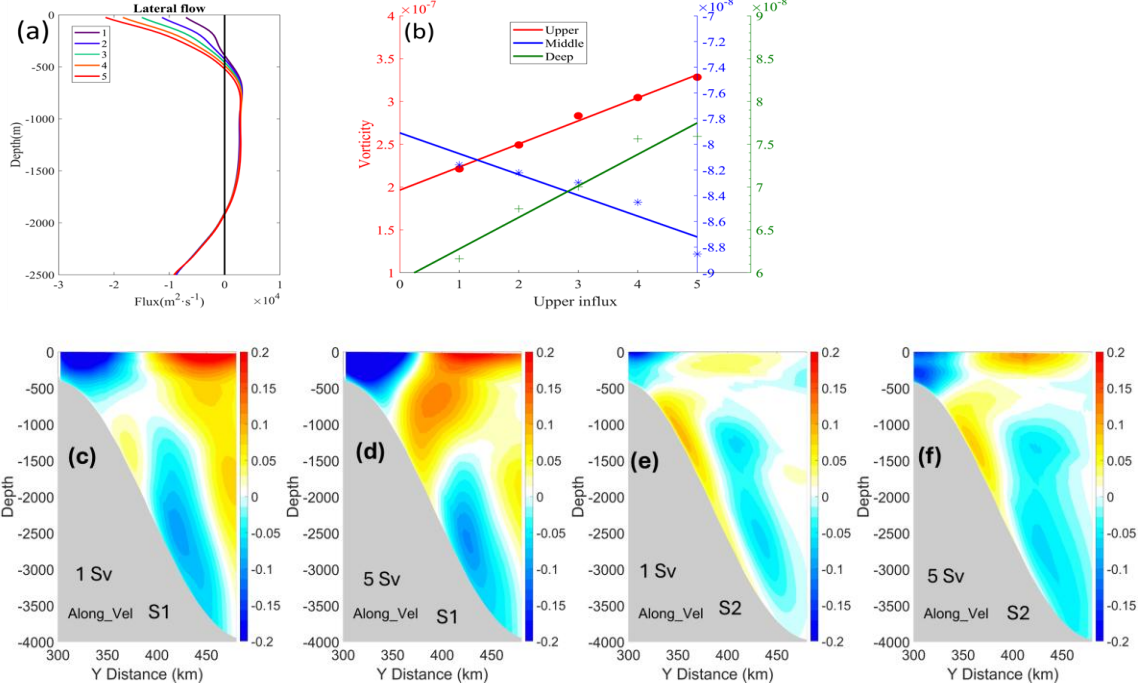
153

154 Figure 3. (a) Vertical profile of domain averaged density ρ ($\text{kg}\cdot\text{m}^{-3}$) in SCS and Pacific between
 155 1000m to 3000m. (b) Black line shows the vertical profile of the SCS basin-averaged vorticity
 156 (s^{-1}) and the red line shows the flux through LS ($\text{m}^2\cdot\text{s}^{-1}$). The positive/negative vorticity
 157 represents the cyclonic/anticyclonic circulation, and the positive/negative value flux represents
 158 the outflux/influx through LS.

159

160

161 To investigate how the changes in upper layer current modulates the layered circulation,
 162 additional numerical experiments were conducted by adjusting the northeastern outflux to 22Sv,
 163 23Sv and 24Sv, thus the upper LS intrusion was adjusted to 3Sv (Case_U3), 2Sv (Case_U2)
 164 and 1Sv (Case_U1). In these scenarios, the middle and deep exchanging currents, which were
 165 primarily sustained by the contrasting densities between the SCS and the open ocean, remained
 166 relatively unchanged (Figure 4a). Inside the basin, the enhancement of the upper layer inflow
 167 directly intensified the upper layer cyclonic circulation (Figure 4 c-f). And subsequently
 168 strengthened the middle anticyclonic slope current, particularly in the northwestern part of the
 169 basin (transect S1, Figure 4c, d). Additionally, although not directly connected to the upper
 170 layer, the deep cyclonic slope current also exhibited increased strength (Figure 4c-f). Using the
 171 domain-averaged vorticity as an indicator, it was observed that the intensification of the upper
 172 layer circulation resulted in a 10% increase in the intensity of the middle anticyclonic
 173 circulation and a 27% increase in the deep cyclonic circulation (Figure 4b). Given that only the
 174 upper layer circulation is directly amplified by the upper intrusion, the remote influence from
 175 upper layer processes over the basin slope significantly impacts the intensity of the layered
 176 circulation, which was explored below.



177

178

179

180 **Figure 4.** (a) Vertical profile flux across the LS under varying upper layer influx. (b) Changes
 181 in the basin-averaged vorticity between 0-500 m (Upper), 1000-2000 m (Middle) and 3000-
 182 4000 m (Deep) with different upper influx. (c-f) The along-slope current ($m \cdot s^{-1}$) over the
 183 section S1 and S1 in Standard case (upper intrusion is 5 Sv) and Case_U1 (upper LS intrusion
 184 is 1Sv), respectively. The locations of the two transects are shown in Figure 1a. The transect
 185 locations are indicated in Figure 1a. Positive values represent anticyclonic flow, while negative
 186 values indicate cyclonic flow.

187

188

189 4. Discussion

190

191 To understand how the upper layer processes modulate the layered current over the slope,
 192 we first investigated the layered-integrated vorticity budget for each layer (Gan, Liu et al. 2016,
 193 Cai, Chen et al. 2023):

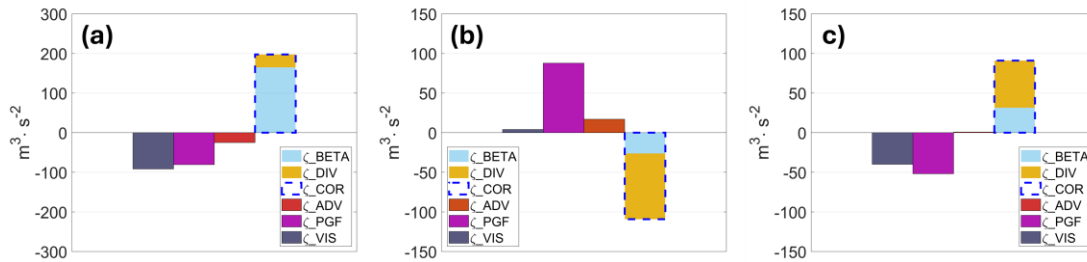
$$\begin{aligned}
 & \overbrace{\int_A [\nabla \times \int_{H_1}^{H_2} (\overrightarrow{PGF}) dz] dA}^{\zeta_PGF} + \overbrace{\int_A [\nabla \times \int_{H_1}^{H_2} (\overrightarrow{ADV}) dz] dA}^{\zeta_ADV} + \overbrace{\int_A [-f \nabla \cdot \int_{H_1}^{H_2} (\overrightarrow{V}_h) dz] dA}^{\zeta_COR} + \overbrace{\int_A [-\beta \cdot \int_{H_1}^{H_2} (v) dz] dA}^{\zeta_BETA} \\
 & \overbrace{\int_A [\nabla \times \int_{H_1}^{H_2} (\overrightarrow{VIS}) dz] dA}^{\zeta_VIS} = 0 \quad (1)
 \end{aligned}$$

196 where \overrightarrow{PGF} is pressure gradient force, \overrightarrow{ADV} is nonlinear advection, \overrightarrow{VIS} is the turbulent
 197 viscosity. The horizontal viscosity is much smaller than vertical viscosity term and they are
 198 included in the \overrightarrow{VIS} term for simplicity. COR is the Coriolis force and the domain-integrated
 199 ζ_COR represents the lateral planetary vorticity flux. The H_1 and H_2 represent the bottom and
 200 upper depth of each layer, respectively. Inside the basin, the ζ_COR can be further decomposed
 201 into the vertical stretching induced by the divergence of the horizontal flow (ζ_DIV) and β

202 effect of the meridional current (ζ_BETA).

203 The circulation in SCS is primarily governed by geostrophic balance, manifested as
 204 ζ_COR balanced by the ζ_PGF in both layers. It suggests that the mean cyclonic/anticyclonic
 205 circulation is related to the lateral planetary vorticity influx/outflux (Figure 5) (Cai and Gan
 206 2019, Cai, Chen et al. 2023; Zhu et al., 2017, 2019). Consequently, the strengthening of the
 207 upper LS intrusion directly intensifies the upper layer cyclonic slope current by providing more
 208 positive planetary vorticity flux. In the semi-enclosed middle and deep layers, the vorticity
 209 input is mainly provided by the ζ_DIV , as also highlighted in the previous studies (Zhu, Sun et
 210 al. 2017, Wang, Du et al. 2018, Cai, Chen et al. 2023). The positive ζ_DIV in the upper and
 211 deep layers reflects the downward and upward flux, which squeeze the middle layer and provide
 212 the negative vertical flux (negative ζ_DIV) for the anticyclonic circulation. Therefore, the
 213 intensification of the middle and deep slope currents is largely attributed to vertical stretching
 214 over the basin slope.

215



216

217

218 **Figure 5.** The layered-integrated vorticity budget (Equation 1) for the standard case in the layers of (a)
 219 0–500, (b) 1,000–2,000, and (c) 2,500–4,000 m.

220

221

222 a. Intensification of middle anticyclonic slope current

223

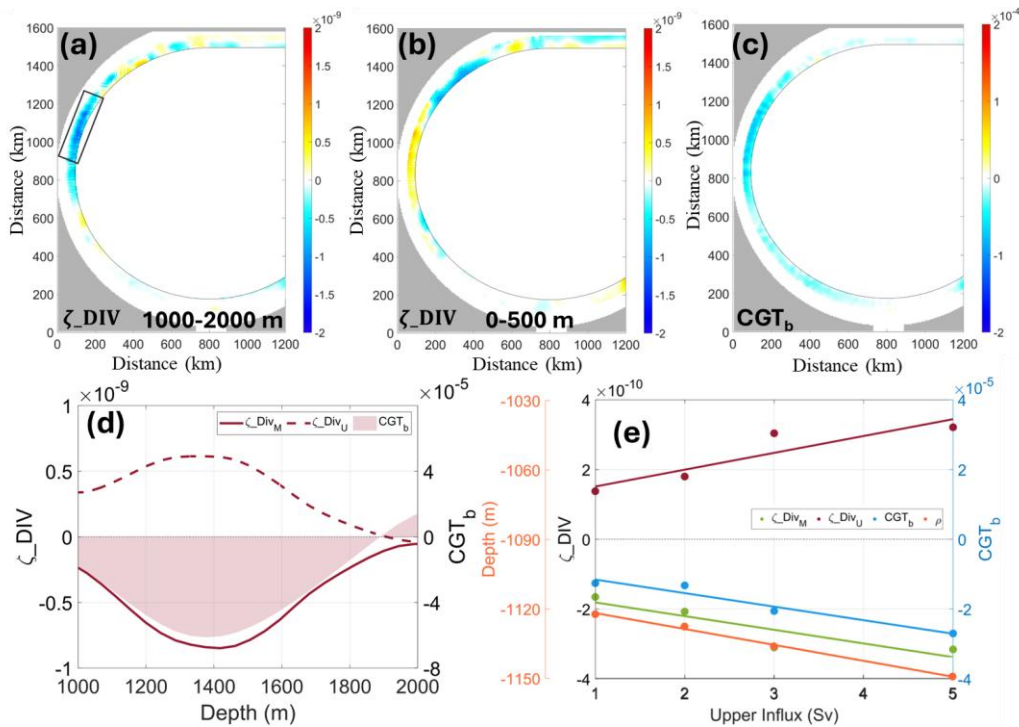
224 For the middle anticyclonic slope current, the negative middle-layered ζ_DIV (ζ_DIV_M) mainly
 225 occurs over the northwestern slope (Figure 6a), where a relatively strong anticyclonic slope
 226 current is observed. In this area, the upper layer generally exhibits positive ζ_DIV (ζ_DIV_U),
 227 indicating downward squeezing from the upper layer that helps maintain the middle
 228 anticyclonic slope current (Figure 6 b). The increased squeezing from the upper slope current
 229 is expected to intensify the middle anticyclonic slope current (Figure 4 c, d). Since the
 230 stretching/squeezing imposed on the slope current is closely related to the vertical motion
 231 (Liang, Spall et al. 2017), the mean vertical motions over the slope can be understood as follows:

$$232 \quad \bar{w} = -\nabla_h \cdot \int_{-H}^Z \vec{V}_h dz \approx -\nabla_h \cdot \int_{-H}^Z \vec{V}_{h_geo} dz - \nabla_h \cdot \int_{-H}^Z \vec{V}_{h_vis} dz$$

$$233 \quad = -\overbrace{(\bar{v}_{b_geo}H_y + \bar{u}_{b_geo}H_x)}^{CGT_b} + \underbrace{\frac{\beta}{f} \int_{-H}^z \bar{v}_{geo} dz - \nabla_h \cdot \int_{-H}^z \bar{\vec{V}}_{h_vis} dz}_{\beta \text{ effect}} \quad (2)$$

234 where H is the topography, $_geo$ represents the geostrophic component of the horizontal
 235 current, which is maintained by the distribution of bottom pressure. $_vis$ represent the vertical
 236 viscosity component. H_x and H_y are the horizontal gradients of the bottom slope, \bar{u}_{b_geo} and
 237 \bar{v}_{b_geo} are the bottom geostrophic currents. When the current flows over the slope, the bottom
 238 pressure distribution interacts with the curved topography and the resulting geostrophic cross-
 239 isobath transport (CGT_b) to influence the vertical motions over the slope. The $Fric$ represent
 240 the effect of the bottom Ekman pumping that induced by the bottom stress of the slope current.
 241 Generally, the CGT_b largely governs the mean vertical motion over northwestern slope, which
 242 in turn squeezes and stretches the middle and upper slope currents. This process is crucial in
 243 maintaining the vorticity input through ζ_DIV (Figure 6 d), thereby sustaining the dynamics of
 244 the slope currents.

245 Associated with the intensification of the upper layer cyclonic slope current, the stronger
 246 slope current modulates the bottom pressure distribution over the slope, leading to stronger
 247 vertical squeezing (ζ_DIV) within the water column. The increase in squeezing gradually
 248 deepens the isopycnal surface and strengthens the middle anticyclonic slope current (Figure 6e).
 249



250

251 **Figure 6.** (a-c) ζ_DIV integrated between 1000-2000 m (ζ_DIV_M), 0-500 m (ζ_DIV_U), and
 252 CGT_b over the region of middle anticyclonic slope current between 1000-2000 m. The black
 253 line indicates the 2000 m isobath line. (d) Change of the ζ_DIV integrated between 100-2000 m

254 (ζ_{DIV_M}), between 0-500 m (ζ_{DIV_U}) with the depth over the northwestern slope. (e) Changes
 255 of the ζ_{DIV_M} , ζ_{DIV_U} , CGT_b and the depth of isopycnal surface of 1027.4 kg/m^3 with different
 256 upper LS influx. (d) and (e) was plotted using the data averaged over the region of black box
 257 in (a)

258

259

260 **b. Intensification of the deep cyclonic slope current**

261 For the deep cyclonic slope current, the deep ζ_{DIV} (ζ_{DIV_D}) features a downward flux
 262 (negative value) over the northern slope and upward flux (positive value) over the southern part
 263 (Figure 7a, d). It suggests the sinking from the northern basin and upwelling from the southern
 264 basin would sustain the abyssal cyclonic circulation. Same as the middle anticyclonic slope
 265 current, the ζ_{DIV_D} is. For the deep layer, the viscosity term has an important effect in the
 266 vorticity budget (Figure 5c). Similarly, the $Fric_D$ term contributes to the deep ζ_{DIV_D} and is
 267 characterized by a relatively uniform downward motion (Figure 7d). However, the primary
 268 pattern and magnitude of the ζ_{DIV_D} are largely controlled by the CGT_b that the pressure
 269 distribution maintained the mean downwelling in the northern side and the upwelling over the
 270 southern slope (Figure 7b, d). Since the $Fric_D$ is induced by the bottom frictional stress as
 271 response to the deep layer slope current, while the bottom pressure is modulated by the motions
 272 of water in the entire water column above it, we further examine the maintenance of the bottom
 273 pressure over the slope.

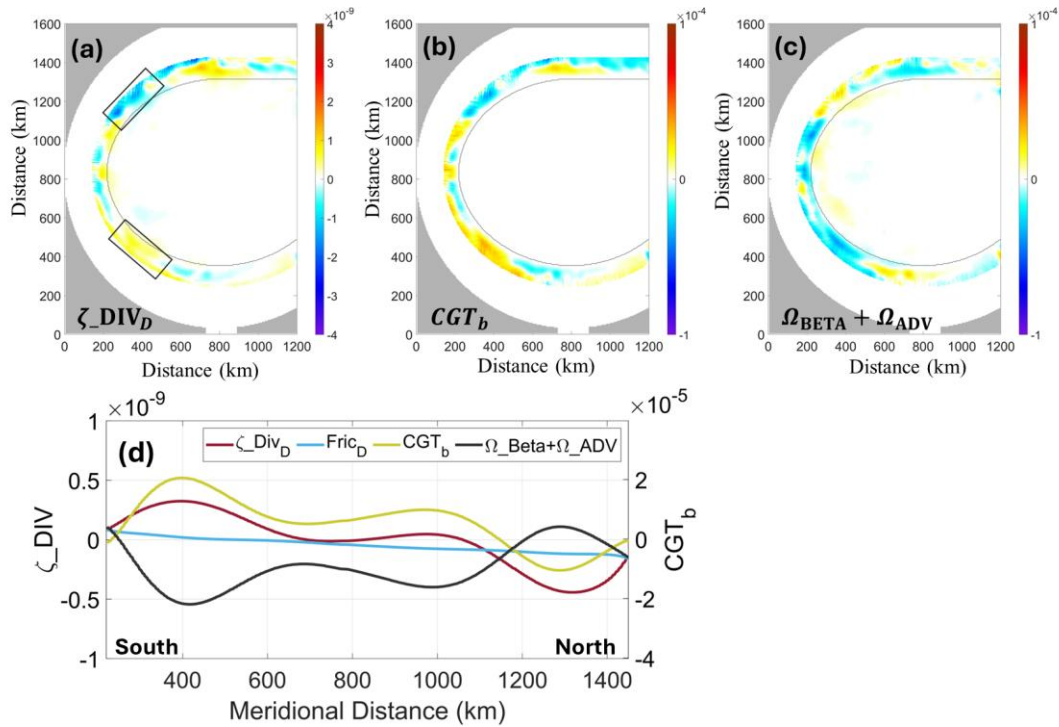
274 To explain the maintenance of the bottom pressure distribution, the vertical integrated
 275 vorticity dynamic was employed (Gan, Liang et al. 2013, Cai and Gan 2021):

$$276 \quad \overbrace{\nabla \times \int_{-H}^0 (\overline{PGF}) dz}^{\Omega_{PGF}} + \overbrace{\nabla \times \int_{-H}^0 (\overline{ADV}) dz}^{\Omega_{ADV}} + \underbrace{\beta \int_{-H}^0 v dz}_{\Omega_{BETA}} - \overbrace{\nabla \times \int_{-H}^0 (\overline{VIS}) dz}^{\Omega_{VIS}} = 0 \quad (3)$$

277 Where $\Omega_{PGF} = \nabla \times \int_{-H}^0 (\overline{PGF}) dz = -(\tilde{v}_{b_geo} H_y + \tilde{u}_{b_geo} H_x)$, thus represents the effect of CGT_b .

278 It illustrates that the bottom pressure distribution is maintained by the nonlinear advection of
 279 relative vorticity (Ω_{ADV}), advection of planetary vorticity (Ω_{BETA}), and net viscosity of the
 280 current flowing over the slope topography. Among them, the Ω_{BETA} and Ω_{ADV} play the
 281 major role in sustaining the bottom pressure distribution of the deep cyclonic slope current
 282 (Figure 8 c, d).

283



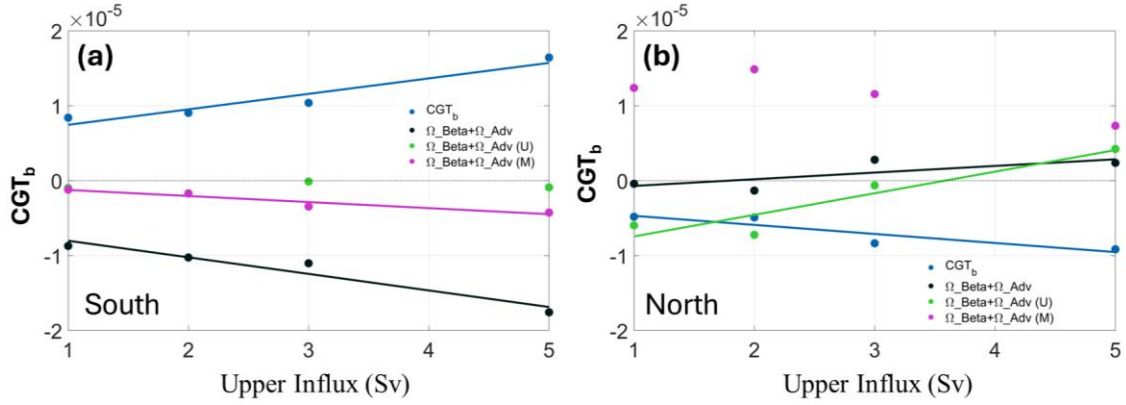
284

285 Figure 7 (a-c) ζ_{DIV} integrated below 3000 m of the deep cyclonic slope current (ζ_{DIV_D}),
 286 CGT_b and $\Omega_{BETA} + \Omega_{ADV}$ over the region of middle anticyclonic slope current below 3000
 287 m. The black line indicates the 4000 m isobath line. (d) Meridional changes of the ζ_{DIV_D} ,
 288 $Fric_D$, CGT_b and $\Omega_{BETA} + \Omega_{ADV}$ over the slope.
 289

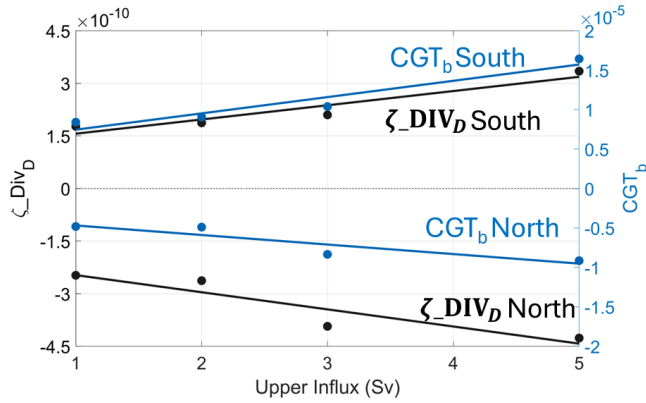
290

As the upper intrusion intensifies, the bottom pressure distribution adjusts in response to
 291 changes in the layered circulation, resulting in a gradual strengthening of the negative
 292 CGT_b over the northern slope and positive CGT_b over the southern part (Figure 8 a-b). Over the
 293 southern slope (Figure 8a), the strengthening of the positive CGT_b is induced by the increase of
 294 the $\Omega_{BETA} + \Omega_{ADV}$ in the water column, in which the middle layer [$\Omega_{BETA} + \Omega_{ADV}$ (M)]
 295 provides approximately 40% of the total strengthening trend, while the upper layer [Ω_{BETA}
 296 + Ω_{ADV} (U)] has a negligible impact. Conversely, over the northern slope, the strengthening
 297 of the $\Omega_{BETA} + \Omega_{ADV}$ is primarily influenced by the upper layer, with the middle layer has
 298 the negative effect (Figure 8b). Thus, the intensification of downward CGT_b over the northern
 299 slope is directly modulated by the strengthening of the upper cyclonic slope current, while the
 300 intensification of upward CGT_b over the southern slope is mainly driven by the strengthening
 301 of the middle anticyclonic slope current. These changes in CGT_b enhance deep stretching,
 302 thereby strengthening the deep cyclonic slope current accordingly (Figure 8c).

303



304



305

306

307 **Figure 8.** (a) Changes of the CGT_b , $\Omega_{Beta} + \Omega_{Adv}$ in the total water column, $\Omega_{Beta} + \Omega_{Adv}$ in the
 308 layer between 0-500 m ($\Omega_{Beta_U} + \Omega_{Adv_U}$), $\Omega_{Beta} + \Omega_{Adv}$ in the between 1000-2000 m
 309 ($\Omega_{Beta_M} + \Omega_{Adv_M}$) over the southern slope (black box in Figure 8a). (b) same as (a) but over
 310 the northern slope (black box in Figure 8a). (c) Change of the CGT_b and ζ_{DIV_D} over the
 311 northern and southern slope.
 312

313

314 5. Summary

315 Marginal sea circulation plays a crucial role in mass transport and regional climate
 316 dynamics. Through process-oriented numerical simulations, we examined how upper-layer
 317 processes, which are characterized by greater intensity and variability, impact the layered
 318 circulation over the curved bottom slope in SCS. The primary goal of our study is to provide
 319 theoretical insights into the mechanisms driving layered circulation and their response to
 320 changes in upper-layer motions. The results underscore the intricate balance between
 321 topographical features and oceanic circulation. These insights have broad applicability to
 322 understanding similar processes and phenomena in other regions, and help to predict the
 323 behavior of marginal sea circulation under varying forcings conditions.

324 The numerical experiments show that the simulated layered exchange currents through the
 325 LS introduce lateral planetary vorticity flux and facilitate the development of a layered basin

326 circulation within the SCS. Inside the basin, the intensification of upper-layer inflow directly
327 enhances the upper-layer cyclonic circulation, which in turn strengthens the middle anticyclonic
328 slope current, particularly in the northwestern part of the basin. Furthermore, even though the
329 deep cyclonic slope current is not directly connected to the upper layer, it also exhibits increased
330 strength. Using domain-averaged vorticity as an indicator, it was found that the intensification
331 of the upper-layer circulation resulted in the increase in the intensity of the middle anticyclonic
332 circulation and deep cyclonic circulation.

333 The vorticity dynamics illustrate that the changes in the middle and deep slope current is
334 largely related to the vertical stretching over the slope (ζ_{DIV}). When the current flows over
335 the slope, the bottom pressure distribution interacts with the curved topography and the
336 resulting geostrophic cross-isobath transport (CGT_b) influences the vertical motions. For the
337 middle anticyclonic slope current, the negative middle ζ_{DIV} predominantly occurs over the
338 northwestern slope, where a relatively strong anticyclonic slope current is present. As the upper-
339 layer cyclonic slope current intensifies, it modulates the bottom pressure distribution over the
340 slope, providing stronger vertical squeezing ζ_{DIV} within the water column, which gradually
341 strengthens the middle anticyclonic slope current. For the deep cyclonic slope current, the deep
342 ζ_{DIV} is also largely controlled by the CGT_b over the slope, with the pressure distribution
343 maintaining downwelling flows in the northern part and upwelling over the southern slope.
344 Over the southern slope, the strengthening of the positive CGT_b is induced by the increase of
345 the nonlinear advection of relative vorticity and planetary vorticity in the entire water column,
346 in which the middle layer provides approximately 40% of the total strengthening trend, while
347 the upper layer has a negligible impact. Conversely, on the northern slope, the strengthening
348 of the negative CGT_b is primarily influenced by the upper layer, with the middle layer has the
349 negative effect. The results from this process-oriented study deepen understanding of the
350 intricate balance between topographical features and layered circulation, which help to improve
351 the predictions of the long-term behavior of marginal sea circulation under varying climatic
352 conditions. It should be noted that those understandings are based on process-oriented
353 simulation with simplified configurations. In the following analysis, a more realistic simulation
354 will provide more quantitative insights into the topographic modulation on the layered
355 circulation in the marginal seas. In addition to the processes revealed in this study, other
356 mechanisms, such as the Neptune Effect involving the eddy-slope interaction (e.g., Holloway,
357 1987, Stewart et al., 2024), may also play a role in influencing circulation dynamics in marginal
358 seas like the SCS. It will be incorporated into our future investigations to improve
359 understanding.

360

361

362 Data availability. All data used in this paper are available at
363 <https://doi.org/10.5281/zenodo.13835538>. The source code can be obtained upon request from
364 the corresponding author.

365

366 Author contributions. QT conducted the investigation, developed the methodology, and carried
367 out the writing (original draft preparation). ZC was responsible for the conceptualization,
368 supervision, and writing (review and editing). ZL was responsible for the conceptualization and
369 writing (review and editing).

370

371 Competing interests. The contact author has declared that none of the authors has any
372 competing interests.

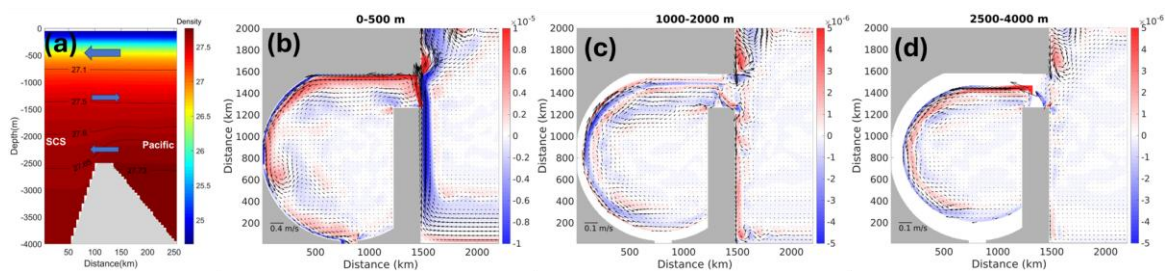
373

374

375 *Acknowledgement*

376 This work was supported by National Natural Science Foundation of China
377 (42376024, 42276004), the Science and Technology Development Fund, Macau SAR
378 (File/Project no. 001/2024/SKL), and The Center for Ocean Research in Hong Kong
379 and Macau (CORE, EF014/FST-CZY/2023/HKUST). The work described in this paper
380 was substantially supported by a grant from the Research Grants Council of the Hong
381 Kong Special Administrative Region, China (AoE/P-601/23-N). CORE is a joint
382 research centre for ocean research between Laoshan Laboratory and HKUST. This
383 work was performed in part at the SICC, which is supported by the SKL-IOTSC,
384 University of Macau.

385



386

387 Figure S1. (a) Vertical transect of density (represented by color shading and contour lines)
388 across the Luzon Strait. The left side represents the SCS basin, while the right side corresponds
389 to the Pacific basin. Schematic arrows indicate the direction of the exchange flow between the
390 two basins. (b-c) The horizontal circulation (arrows) and depth averaged vorticity (color) of (b)
391 upper layer 0-500 m, (c) middle layer 1000-2000 m and (d) deep layer 2500-4000 m in the
392 standard case.

393

394 **Reference**

395 Cai, Z., D. Chen and J. Gan (2023). "Formation of the Layered Circulation in South China Sea With the Mixing
396 Stimulated Exchanging Current Through Luzon Strait." Journal of Geophysical Research: Oceans **128**(3).

397 Cai, Z. and J. Gan (2019). "Coupled External-Internal Dynamics of Layered Circulation in the South China Sea: A
398 Modeling Study." Journal of Geophysical Research: Oceans **124**(7): 5039-5053.

399 Cai, Z. and J. Gan (2021). "Dynamics of the Layered Circulation Inferred from Kinetic Energy Pathway in the South
400 China Sea." Journal of Physical Oceanography **51**(5): 1671-1685.

401 Gan, J., H. Kung, Z. Cai, Z. Liu, C. Hui and J. Li (2022). "Hotspots of the stokes rotating circulation in a large
402 marginal sea." Nat Commun **13**(1): 2223.

403 Gan, J., H. Li, E. N. Curchitser and D. B. Haidvogel (2006). "Modeling South China Sea circulation: Response to
404 seasonal forcing regimes." Journal of Geophysical Research **111**(C6).

405 Gan, J., L. Liang and H. San Ho (2013). "Dynamics of Intensified Downwelling Circulation over a Widened Shelf
406 in the Northeastern South China Sea." Journal of Physical Oceanography **43**(1): 80-94.

407 Gan, J., Z. Liu and C. R. Hui (2016a). "A Three-Layer Alternating Spinning Circulation in the South China Sea."
408 Journal of Physical Oceanography **46**(8): 2309-2315.

409 Gan, J., Z. Liu, and L. Liang, Numerical modeling of intrinsically and extrinsically forced seasonal circulation in the
410 China Seas: A kinematic study. Journal of Geophysical Research: Oceans, 2016b. 121(7): p. 4697-4715.

411 Holloway (1987): Systematic forcing of large-scale geophysical flows by eddy-topography interaction, Journal of
412 Fluid Mechanics.

413 Johns, W. E. and S. S. Sofianos (2012). "Atmospherically Forced Exchange through the Bab el Mandeb Strait."
414 Journal of Physical Oceanography **42**(7): 1143-1157.

415 Lan, J., Y. Wang, F. Cui and N. Zhang (2015). "Seasonal variation in the South China Sea deep circulation." Journal
416 of Geophysical Research: Oceans **120**(3): 1682-1690.

417 Lan, J., N. Zhang and Y. Wang (2013). "On the dynamics of the South China Sea deep circulation." Journal of
418 Geophysical Research: Oceans **118**(3): 1206-1210.

419 Liang, X., M. Spall and C. Wunsch (2017). "Global Ocean Vertical Velocity From a Dynamically Consistent Ocean
420 State Estimate." Journal of Geophysical Research: Oceans **122**(10): 8208-8224.

421 Millot, C. (1999). "Circulation in the western Mediterranean Sea." Journal of Marine Systems **20**(1-4): 423-442.

422 Nan, F., Xue, H. and Yu, F., 2015. Kuroshio intrusion into the South China Sea: A review. Progress in Oceanography,
423 137, pp.314-333.

424 Oey, L., T. Ezer and H. Lee (2005). "Loop Current, rings and related circulation in the Gulf of Mexico: A review of
425 numerical models and future challenges." Geophysical Monograph-American Geophysical Union **161**: 31.

426 Olvera-Prado, E. R., E. Moreles, J. Zavala-Hidalgo and R. Romero-Centeno (2023). "Upper-Lower Layer Coupling
427 of Recurrent Circulation Patterns in the Gulf of Mexico." Journal of Physical Oceanography **53**(2): 533-550.

428 Omstedt, A., J. Elken, A. Lehmann and J. Piechura (2004). "Knowledge of the Baltic Sea physics gained during the
429 BALTEX and related programmes." Progress in Oceanography **63**(1-2): 1-28.

430 Quan, Q. and H. Xue (2018). "Layered model and insights into the vertical coupling of the South China Sea
431 circulation in the upper and middle layers." Ocean Modelling **129**: 75-92.

432 Shchepetkin, A. F. and J. C. McWilliams (2005). "The regional oceanic modeling system (ROMS): a split-explicit,
433 free-surface, topography-following-coordinate oceanic model." Ocean Modelling **9**(4): 347-404.

434 Shu, Y., Q. Wang and T. Zu (2018). "Progress on shelf and slope circulation in the northern South China Sea."
435 Science China Earth Sciences **61**(5): 560-571.

436 Shu, Y., H. Xue, D. Wang, F. Chai, Q. Xie, J. Yao and J. Xiao (2014). "Meridional overturning circulation in the
437 South China Sea envisioned from the high-resolution global reanalysis data GLBa0.08." Journal of Geophysical
438 Research: Oceans **119**(5): 3012-3028.

439 Song, Y. and D. Haidvogel (1994). "A semi-implicit ocean circulation model using a generalized topography-
440 following coordinate system." Journal of Computational Physics **115**(1): 228-244.

441 Stewart et al. (2024): Formation of eastern boundary undercurrents via mesoscale eddy rectification, Journal of
442 Physical Oceanography.

443 Tenreiro, M., J. Candela, E. P. Sanz, J. Sheinbaum and J. Ochoa (2018). "Near-Surface and Deep Circulation
444 Coupling in the Western Gulf of Mexico." Journal of Physical Oceanography **48**(1): 145-161.

445 Tian, J., Q. Yang and W. Zhao (2009). "Enhanced diapycnal mixing in the South China Sea." Journal of Physical
446 Oceanography **39**(12): 3191-3203.

447 Wang, A., Y. Du, S. Peng, K. Liu and R. X. Huang (2018). "Deep water characteristics and circulation in the South
448 China Sea." Deep Sea Research Part I: Oceanographic Research Papers **134**: 55-63.

449 Wang, G., S.-P. Xie, T. Qu and R. X. Huang (2011). "Deep South China Sea circulation." Geophysical Research
450 Letters **38**(5): n/a-n/a.

451 Yabal, H. (1983). Continental margin geology, Petroleum Industry Press.

452 Yang, Q., W. Zhao, X. Liang and J. Tian (2016). "Three-Dimensional Distribution of Turbulent Mixing in the South

453 China Sea." Journal of Physical Oceanography **46**(3): 769-788.

454 Ye, R., C. Zhou, W. Zhao, J. Tian, Q. Yang, X. Huang, Z. Zhang and X. Zhao (2019). "Variability in the Deep
455 Overflow through the Heng-Chun Ridge of the Luzon Strait." Journal of Physical Oceanography **49**(3): 811-825.

456 Zhang, Z., W. Zhao, J. Tian, Q. Yang and T. Qu (2015). "Spatial structure and temporal variability of the zonal flow
457 in the Luzon Strait." Journal of Geophysical Research: Oceans **120**(2): 759-776.

458 Zhu, Y. and X. Liang (2020). "Coupling of the Surface and Near-Bottom Currents in the Gulf of Mexico." J Geophys
459 Res Oceans **125**(11): e2020JC016488.

460 Zhu, Y., J. Sun, Y. Wang, Z. Wei, D. Yang and T. Qu (2017). "Effect of potential vorticity flux on the circulation in
461 the South China Sea." Journal of Geophysical Research: Oceans **122**(8): 6454-6469.

462 Zhu, Y., Sun, J., Wang, Y., Li, S., Xu, T., Wei, Z. and Qu, T., 2019. Overview of the multi-layer circulation in the
463 South China Sea. *Progress in Oceanography*, 175, pp.171-182.

464 Zhou, C., Xiao, X., Zhao, W. et al. Increasing deep-water overflow from the Pacific into the South China Sea revealed
465 by mooring observations. *Nat Commun* 14, 2013 (2023). <https://doi.org/10.1038/s41467-023-37767-4>

466

467